# A *Drosophila* RNAi screen reveals conserved glioblastoma-related adhesion genes that regulate collective cell migration

Nirupama Kotian[1], Katie M. Troike[2], Kristen N. Curran[1], Justin D. Lathia[2] and Jocelyn A. McDonald[1,*]

[1] Division of Biology, Kansas State University, Manhattan, KS 66506, USA

[2] Lerner Research Institute, Cleveland Clinic, Cleveland, OH 44195, USA

*Correspondence: jmcdona@ksu.edu

116 Ackert Hall, 1717 Claflin Rd., Manhattan, KS 66506

Key Words: *Drosophila,* cell adhesion, collective migration, glioblastoma, *α-catenin*, *Symplekin*, *Lachesin*, *roughest*, *dreadlocks*, *Wnt4*, *dachsous*, *fat*

Running Title: RNAi screen for brain tumor-related migration genes

**ABSTRACT**:

Migrating cell collectives are key to embryonic development but also contribute to invasion and metastasis of a variety of cancers. Cell collectives can invade deep into tissues, leading to tumor progression and resistance to therapies. Collective cell invasion is also observed in the lethal brain tumor glioblastoma, which infiltrates the surrounding brain parenchyma leading to tumor growth and poor patient outcomes. *Drosophila* border cells, which migrate as a small cell cluster in the developing ovary, are a well-studied and genetically accessible model used to identify general mechanisms that control collective cell migration within native tissue environments. Most cell collectives remain cohesive through a variety of cell-cell adhesion proteins during their migration through tissues and organs. In this study, we first identified cell adhesion, cell junction, and associated regulatory genes that are expressed in human brain tumors. We performed RNAi knockdown of the *Drosophila* orthologs in border cells to evaluate if migration and/or cohesion of the cluster was impaired. From this screen, we identified eight adhesion genes that disrupted border cell collective migration upon RNAi knockdown. Bioinformatics analyses further demonstrated that subsets of the orthologous genes were elevated in the margin and invasive edge of human glioblastoma patient tumors. These data together show that conserved cell adhesion and adhesion regulatory proteins with potential roles in tumor invasion also modulate collective cell migration. This dual screening approach for adhesion genes linked to glioblastoma and border cell migration thus may reveal conserved mechanisms that drive collective tumor cell invasion.

## INTRODUCTION

While migrating cells contribute to many processes during embryonic development and adult wound healing, abnormal cell migration drives tumor cell invasion and metastasis. During development and in cancer, cells either migrate as single cells or as interconnected small to large groups of cells called collectives (Friedl and Gilmour 2009; Friedl et al. 2012; Scarpa and Mayor 2016; Te Boekhorst et al. 2016). Especially in cancer, cells can interconvert their modes of movement, transitioning from collective to single cell movement and back (Te Boekhorst and Friedl 2016). A wide variety of cancer cells, including breast, colorectal, and thyroid carcinomas, are now known to migrate and invade as collectives both *in vitro* and *in vivo* (Cheung and Ewald 2016; Wang et al. 2016; Kim et al. 2017; Ilina et al. 2018; Libanje et al. 2019; Padmanaban et al. 2019). Recent work has shown that tumor cell collectives promote tumor invasion and metastasis and may provide a mechanism for resistance to radiation (Aceto et al. 2014; Cheung et al. 2016; Haeger et al. 2019).

The *Drosophila* border cells, which migrate collectively during late oogenesis, are a simple and genetically tractable model to identify genes required for collective cell migration (Montell et al. 2012; Saadin and Starz-Gaiano 2016). The border cell cluster consists of 4-8 epithelial-derived follicle cells that surround a central pair of polar cells (Figure 1, A-C, and F). Individual border cells stay adhered together and their movement is coordinated as an entire unit during the 3- to 4-hour journey to the oocyte (Figure 1, A-C). Multiple studies have used border cells to identify conserved genes that contribute to the migration of a variety of cancer cells, including those that invade as collectives (Yoshida et al. 2004; Madsen et al. 2015; Stuelten et al. 2018; Volovetz et al. 2020).

Glioblastoma (GBM) is the most common primary malignant brain tumor (Ostrom et al. 2014) and is refractory to many therapies including radiation and chemotherapy (Bao et al. 2006, Chen et al. 2012,). Given the dismal prognosis of GBM, identifying the underlying mechanisms that drive progression, including cell invasion, remains an immediate priority. While many genes are known to be dysregulated in glioma patients, it is difficult to know which ones are most relevant to disease progression, including tumor invasion. We and others recently showed that glioma cells and GBM cancer stem cells (CSCs), which can drive tumor growth, migrate collectively in some contexts (Gritsenko et al. 2017; Gritsenko and Friedl 2018; Volovetz et al. 2020). Using several patient derived GBM CSC tumor models, we found that a gene required in border cells, the small GTPase Rap1, also contributes to GBM collective cell invasion (Chang et al. 2018; Sawant et al. 2018; Volovetz et al. 2020). Because patient derived GBM CSC tumor models are less genetically accessible for screening approaches, we have turned to *Drosophila* border cells to identify conserved genes that may drive GBM collective tumor invasion but also may have a more general role in collective cell migration.

Cell-cell and cell-matrix adhesions are critical for cells to stay together and move collectively *in vivo* (Friedl and Mayor 2017; Janiszewska et al. 2020). Thus, genes that regulate cell adhesion are strong candidates to promote collective cell cohesion, migration and invasion. Here we used the border cell system to screen a subset of adhesion and adhesion-related genes that have the potential to regulate GBM tumor migration and invasion. We selected conserved adhesion genes, genes associated with cell junctions, and genes that regulate cell-cell adhesion. We further focused on those adhesion-related genes whose expression correlated with glioma patient survival but at the time of the screen did not have known functions in brain cancer. We performed an RNAi screen targeting 23 of these adhesion genes in border cells. Here, we report the identification of

eight genes, *α-catenin* (*α-Cat*), *Symplekin* (*Sym*), *Lachesin* (*Lac*), *roughest* (*rst*), *dreadlocks* (*dock*), *Wnt4*, *dachsous* (*ds*), and *fat* (*ft*), whose knockdown disrupted border cell migration and/or cluster cohesion to differing degrees. We then identified three human orthologs of target genes that were enriched in the leading edge and invasive portion of GBM tumors, the α-Cat ortholog CTNNA2, the Lac ortholog NEGR1, and the Rst ortholog KIRREL3. While further work needs to be done to test these genes in GBM tumors, this study supports the use of *Drosophila* genetic approaches to provide insights into human diseases such as GBM.

## METHODS & MATERIALS

### Identification of candidate genes

FlyBase FB2014_5 version (released September 9, 2014) was queried for adhesion genes using the following Gene Ontology (GO) controlled vocabulary (CV) terms: 'apical junction complex', 'focal adhesion', 'cell adhesion molecule binding', 'cell junction maintenance', 'cell junction assembly', and 'cell-cell adherens junction'. A total of 133 *Drosophila* genes were identified. Human orthologs were identified by *Drosophila* RNAi Screening Center Integrative Ortholog Prediction Tool (DIOPT) scores (Hu et al. 2011; Table 1). A PubMed search was performed for these genes along with 'glioma', 'glioblastoma', or 'brain cancer' to eliminate genes with a known function in or association with these cancers. This step narrowed the list to 44 genes. The NCBI REMBRANDT database was next used to identify genes that are associated with brain cancer patient survival; these results were then confirmed using The Cancer Genome Atlas (TCGA). Genes associated with better ("positive"), or worse ("negative") patient survival were selected. These analyses resulted in 23 conserved fly genes (34 human genes) that were the final candidate genes tested in the *in vivo* border cell RNAi screen.

110

111 **Bioinformatics analyses of human genes in tumor databases**

112 Regional gene expression data from GBM tumor tissue was obtained from the Ivy Glioblastoma
113 Atlas Project (Ivy GAP) database (https://glioblastoma.alleninstitute.org/static/home, accessed
114 June 20, 2021), which contains gene expression data from several anatomical features of GBM
115 tumors in a 41 patient dataset. Analysis of gene expression based on glioma grade (grades II, III,
116 and IV) was performed using The Cancer Genome Atlas (TCGA) data downloaded from the
117 Gliovis data portal (http://gliovis.bioinfo.cnio.es/, accessed May 5, 2021). The GEPIA (Gene
118 Expression Profiling Interactive Analysis; http://gepia.cancer-pku.cn/, accessed March 30, 2021)
119 database (Tang et al. 2017) was used to compare differential expression of gene orthologs in GBM
120 tumor tissue (n=163) and non-tumor brain tissue (n=207). Thresholds were set at a log2 fold
121 change > 1 and a p value < 0.01.

122

123 ***Drosophila* RNAi Screen and Genetics**

124 All genetic crosses were set up at 25°C. The tub-GAL80ts ('tsGAL80') transgene (McGuire et al.,
125 2004) was included to prevent early GAL4-UAS expression and potential lethality at larval or
126 pupal stages of development. *c306*-GAL4, tsGal80*;* Sco/CyO was used to drive UAS-RNAi line
127 expression in border cells. UAS-mCherry RNAi crossed to c306-GAL4 tsGal80*;* Sco/CyO was
128 used as a control. The expression pattern of *c306*-GAL4 was confirmed by crossing *c306*-GAL4,
129 tsGal80*;* Sco/CyO to UAS-nls.GFP (BDSC 4776). Multiple RNAi lines for the 23 cell adhesion
130 candidate genes and UAS-mCherry RNAi were obtained from the Vienna Drosophila RNAi
131 Center (VDRC) or the Harvard Transgenic RNAi Project (TRiP) collection from the Bloomington
132 Drosophila Stock Center (BDSC). All lines with stock numbers and construct IDs are listed in

Table 2. Males from each UAS-RNAi line were crossed to virgin c*306*-GAL4, tsGal80 females. Three-to-five-day old F1 progeny females (*c306*-GAL4, tsGAL80/+; +/UAS-RNAi) from these crosses were fattened on wet yeast paste for ≥14 hours at 29°C prior to dissection. This allowed maximum GAL4-UAS expression and full inactivation of tsGAL80. Each RNAi line was tested one time in the primary screen, with a subset of lines tested at least three times in the secondary screen unless otherwise noted (Table 2).

**Immunostaining and Imaging**

Ovaries were dissected in Schneider's *Drosophila* Medium (Thermo Fisher Scientific, Waltham, MA, USA). After dissection, ovaries were fixed in 4% formaldehyde (Polysciences, Inc., Warrington, PA, USA) in 0.1 M potassium phosphate buffer, pH 7.4 for 10 minutes. NP40 block (50 mM Tris-HCl, pH 7.4, 150 mM NaCl, 0.5% NP40, 5 mg/ml bovine serum albumin [BSA]) was used for intermediate washes and antibody dilutions. Primary antibodies were obtained from Developmental Studies Hybridoma Bank (DSHB, University of Iowa, Iowa City, IA, USA) and used at the following dilutions: rat monoclonal anti-E-Cadherin 1:10 (DCAD2), mouse monoclonal anti-Armadillo 1:100 (N27A1), and mouse monoclonal anti-Singed 1:25 (Sn7C). Anti-rat or isotype-specific anti-mouse secondary antibodies conjugated to Alexa Fluor-488 or -568 (Thermo Fisher Scientific) were used at 1:400 dilution. 4',6-Diamidino-2-phenylindole (DAPI, Millipore Sigma) was used at 2.5µg/ml to label nuclei. Aqua-Poly/Mount (Polysciences, Inc.) was used to mount egg chambers on slides, a coverslip was added, and the mounting media allowed to harden for three days prior to microscope imaging. The stained egg chambers were imaged either using an upright Zeiss AxioImager Z1 microscope with Apotome.2 optical sectioning or on a Zeiss LSM 880 confocal microscope (KSU College of Veterinary Medicine

Confocal Core), using a 20x 0.75 numerical aperture (NA) objective. Images were processed in Zeiss ZEN 2 or FIJI software. Figures were prepared in Adobe Photoshop 2021 and line drawings were made in Adobe Illustrator 2021.

**Graphs and statistics**

Graphs were prepared in GraphPad Prism 8 (GraphPad Software, San Diego, CA, USA). For the secondary screen and subsequent analyses, three trials were performed for each RNAi line ($n \geq 30$ egg chambers scored in each trial). The cutoff value for a migration defect was calculated based on the background mean migration defect (3% ± 0.02) in control egg chambers (*c306*-GAL4 tsGAL80/+; +/UAS-mCherry RNAi). To determine genuine "hits" from the screen, RNAi lines with ≥10% migration defects were scored as positive hits in the primary and secondary screens. P-values were calculated using an unpaired two-tailed t test in Microsoft Excel. For GBM regional and grade-dependent gene expression analyses, differences between groups were determined using a one-way ANOVA. N's and p-values for each trial are included in the figure legends and tables.

**Data Availability**

Strains are available upon request. The authors affirm that all data necessary for confirming the conclusions of the article are present within the article, figures, and tables. Table 2 contains the complete results of the screen, including the RNAi lines tested, availability from the public stock centers (BDSC "BL" and VDRC), and detailed results from the primary and secondary screens. Supplementary Table 1 includes statistics for Figure 4 and Supplementary Figure 1. Supplementary Figure 1 shows the regional expression of the rest of the human orthologs in GBM patient tumors. Supplementary Figure 2 shows the expression of human ortholog adhesion genes

in different glioma tumor grades. Supplementary Figure 3 shows a comparison of human ortholog adhesion gene expression in GBM versus non-tumor brain tissue.

## RESULTS AND DISCUSSION

### Identification of conserved brain tumor-associated adhesion genes

Cell-cell adhesion is essential for cells to stay connected during cohesive collective migration (Friedl and Mayor 2017). Reduction (or loss) of adhesion genes, such as E-cadherin (*Drosophila shotgun* [*shg*]), disrupts the integrity of the cluster and blocks the migration of the border cell cluster to the oocyte (Figure 1, D and E) (Niewiadomska et al. 1999; Sarpal et al. 2012; Desai et al. 2013; Cai et al. 2014; Chen et al. 2020, Raza et al. 2019). Many adhesion genes are conserved from flies to humans and could contribute to both border cell migration and GBM invasion (Figure 1F). To identify these conserved adhesion genes, we first performed a search of the *Drosophila* genome (FB2014_05), using Gene Ontology (GO) controlled vocabulary (CV) terms associated with cell adhesion (see Methods & Materials for details; Figure 1G). From the 133 fly genes associated with one or more of these terms, we identified likely human orthologs by analyzing their DIOPT scores (Table 1; Hu et al., 2011). Using these human orthologs, we performed a PubMed search for those genes to determine if there was an already-known association with either glioma or GBM. This allowed us to focus on genes that may have a novel association with brain tumors. The remaining 44 genes were then analyzed in the Repository of Molecular Brain Neoplasia Data (REMBRANDT), a database for transcript expression levels that are associated with brain tumor patient survival (Gusev et al., 2018). Ten genes were not found in REMBRANDT. Of the remaining 34 human genes, expression of 18 genes (13 fly genes) were associated with better (“positive”) patient survival while expression of 16 genes (13 fly genes) were associated with worse (“negative”) patient survival (Table 1). Many fly genes have multiple

human orthologs. A few of these, for example *α-cat*, *G protein alpha i subunit*, and *G protein alpha o subunit*, have multiple human orthologs each of whose expression is associated with different predicted glioma patient outcomes (Table 1). The 23 unique fly genes were chosen for further follow-up to determine their role, if any, in border cell collective migration.

**RNAi screen in border cells identifies eight genes associated with GBM**

For the primary screen, multiple RNAi lines were used to specifically target and knock down each of the 23 conserved fly adhesion genes in border cells (Table 2). We drove expression of the respective UAS-RNAi lines using *c306*-GAL4 tsGAL80, a follicle cell driver highly enriched in border cells; tsGAL80 was used to bypass early lethality (Figure 1, A-C). All border cell clusters from control (*c306*-GAL4 tsGAL80/+; +/UAS-mCherry RNAi) egg chambers completed their migration by stage 10 (Figure 2, A and B; Table 2). Twenty-one of these genes displayed a migration defect above the minimum cutoff of ≥10% with at least one RNAi line (*see* Methods & Materials).

To further determine which of these genes were genuine hits, we retested the RNAi lines in a secondary screen. Each RNAi line was crossed to *c306*-GAL4 tsGAL80 three times and scored for the ability of border cells to complete their migration to the oocyte. For three genes (*ds, Lac, rst*), additional RNAi lines were obtained and tested. We specifically analyzed if RNAi border cells failed to initiate migration ("no migration"), stopped along the migration pathway but did not reach the oocyte ("partial migration"), reached the oocyte ("complete migration"), or if clusters had defective cohesion and split into multiple parts ("% splitting"). Control border cells completed their migration to the oocyte by stage 10 (Figure 2, A and B; Figure 3, A and B; Table 2). We found that knockdown of eight genes, *α-Cat, Sym*, *Lac, rst*, *dock*, *Wnt4*, *ds*, and *ft*, consistently

disrupted border cell migration with at least two RNAi lines, providing more confidence that these genes are required for collective cell migration (Figures 2 and 3; Table 2). Border cell migration defects upon knockdown of these genes ranged from 10 to 76% depending on the gene and the RNAi line; some RNAi lines for these genes had less than 10% migration defects. Below we report and discuss the results for these eight genes in more detail.

*Adherens junction genes*: α-Cat (human CTNNA1, CTNNA2, CTNNA3) is a critical component of the cadherin-catenin complex that regulates adherens junctions by linking E-cadherin and β-catenin to the F-actin cytoskeleton (Maiden and Hardin 2011). E-cadherin is required for adhesion of border cells to the nurse cell substrate, which provides traction for border cells to keep moving forward and thus facilitates forward movement while maintaining tension-based directional motility (Niewiadomska et al. 1999; Cai et al. 2014). α-Cat was the strongest candidate from our primary screen (Table 2), and we recently described the phenotypes for *α-Cat* knockdown in detail (Chen et al. 2020). *α-Cat* was knocked down using two independent RNAi lines, which reduced α-Cat protein levels in border cells (Chen et al. 2020). *α-Cat* RNAi strongly disrupted migration, with 66-76% border cells failing to complete their migration (Figure 2, C, D and M; Table 2). Border cell clusters deficient for *α-Cat* also had significant cohesion defects, with the cluster splitting into two or more parts in 35% of egg chambers (Figure 2, C and D). Thus, *Drosophila α-Cat* is required for both successful border cell migration and for proper cohesion of cells within the cluster (this study; Sarpal et al. 2012; Desai et al. 2013; Chen et al. 2020). The role for α-Cat in cluster cohesion and migration closely resembles that of β-Cat (*Drosophila* Armadillo) and E-cadherin, thus it is likely that α-Cat functions in the classical cadherin-catenin complex in border cells (Niewiadomska et al. 1999; Sarpal et al. 2012; Desai et al. 2013; Cai et al. 2014; Chen et al. 2020).

*Other junctional genes:* Four genes, *Sym*, *Lac*, *rst*, and *dock*, encode proteins that localize to various types of cell junctions and/or are known to regulate cell adhesions. Sym (human SYMPK) is a scaffolding protein, which along with other polyadenylation factors, forms a complex that mediates processing of polyadenylated and histone mRNAs but also functions at tight junctions (Keon et al. 1996; McCrea et al. 2009; Sullivan et al. 2009). During *Drosophila* oogenesis, Sym is required for histone pre-mRNA processing in the histone locus body during endoreplication of the follicular epithelium (Tatomer et al. 2014). Later in oogenesis, Sym protein localizes to the tricellular junctions of follicle cells. Here, Sym may facilitate cytoplasmic mRNA polyadenylation and thus translation of mRNAs required to regulate and/or maintain adhesion at cell junctions (Tatomer et al, 2014). Border cells expressing *Sym* RNAi had significant migration defects along with splitting of the cluster (Figure 2, E and F, N; Table 2). The two strongest *Sym* RNAi lines (VDRC 33469 and 33470), which target the same region of the *Sym* gene, caused significant migration defects, with 5-10% of border cells failing to start migration and an additional 18-22% failing to reach the oocyte. *Sym* RNAi border cell clusters had cohesion defects, with 11% of clusters visibly splitting apart. A third independent RNAi line (BL 39041) did not impair migration (Figure 2N). Based on our observed phenotypes and the known roles for Sym, we speculate that *Sym* may maintain cell-cell contacts between border cells during collective migration, possibly through regulation of as-yet-unknown targets by mRNA polyadenylation at cell-cell junctions.

Lac (human LSAMP and NEGR1) is a membrane-localized protein with three extracellular immunoglobulin-like (Ig-like) domains that can mediate cell-cell adhesion (Finegan and Bergstralh 2020). Lac localizes to both immature and mature basolateral septate junctions and is required for tracheal morphogenesis in *Drosophila* (Llimargas et al. 2004). Knockdown of *Lac* by four RNAi lines, which together target two non-overlapping regions of the *Lac* gene, mildly

disrupted migration and cluster cohesion (Figure 2, G and H, O; Table 2). Two *Lac* RNAi lines (VDRC 35524 and BL 28940) disrupted migration in 11% of egg chambers, whereas two RNAi lines (VDRC 107450 and BL 38536) had fewer migration defects and were not significantly different from control (Figure 2O; Table 2). While the phenotypes caused by *Lac* RNAi knockdown are mild, *Lac* is likely to be a true regulator of border cell migration. Recent work by Alhadyian et al. found that four additional septate junction proteins, Macroglobulin complement-related (Mcr), Contactin, Neurexin-IV and Coracle, localize to border cells and are required for both border cell cluster migration and cohesion (Alhadyian et al. 2021). Because border cells do not have mature septate junctions (which form the tight occluding junctions), septate junction proteins may instead regulate cluster polarity and/or adhesion during migration (Alhadyian et al. 2021). Further work will be needed to determine if the mild phenotypes observed with *Lac* RNAi are due to partial knockdown or to redundancy with other septate junction genes.

Rst (human KIRREL1, KIRREL2, KIRREL3) is a member of the Irre Cell Recognition Module (IRM) family of transmembrane proteins. In particular, Rst encodes an immunoglobulin superfamily cell adhesion molecule (IgCAM) with five Ig-like domains (Finegan and Bergstralh 2020). IRM proteins, including Rst, control the adhesion and patterning of various tissues including the developing ommatidia in the *Drosophila* eye (Bao and Cagan 2005; Johnson et al. 2011; Finegan and Bergstralh 2020). Border cells expressing *rst* RNAi showed consistent though mild migration defects with three RNAi lines (VDRC 27223, VDRC 27225, and BL 28672), which in total target two non-overlapping regions of the *rst* gene. Migration defects ranged from 10-16% (Figure 2, I and J, P; Table 2). Cluster cohesion was mildly affected (6% of clusters split apart; Figure 2I). A fourth RNAi line did not disrupt migration or cohesion compared to control (Figure 2P; VDRC 951). Interestingly, Rst is required for progression through *Drosophila* adult oogenesis,

including development of the germline (Valer et al. 2018; Ben-Zvi and Volk 2019). Rst is also expressed in follicle cells prior to the stages that border cells develop from the follicle cell epithelium (Valer et al. 2018), further supporting a later role in border cell migration.

Dock (human NCK1) is an SH2/SH3 domain-containing adaptor protein involved in receptor tyrosine kinase signaling, actin regulation, cell adhesion, and other processes (Buday et al. 2002; Chaki and Rivera 2013). In *Drosophila*, Dock regulates axon guidance, myoblast fusion during embryonic development, and ring canal morphogenesis in the ovarian germline-derived nurse cells (Garrity et al. 1996; Rao and Zipursky 1998; Kaipa et al. 2013; Stark et al. 2021). Knockdown of *dock* in border cells, using two independent RNAi lines that target non-overlapping regions of the *dock* gene (VDRC 37524 and BL 27228), resulted in migration defects but did not disrupt cohesion of border cells (Figure 2, K, L, and Q; Table 2). Specifically, *dock* RNAi disrupted migration in 13-19% of stage 10 egg chambers (Figure 2Q; Table 2). One RNAi line (VDRC 107064) did not impair border cell migration but showed mild splitting (6%), whereas another line (VDRC 37525) from the primary screen was no longer available so could not be confirmed in the secondary screen (Figure 2Q; Table 2). Dock is required for myoblast fusion during muscle formation by regulating cell adhesion and F-actin (Kaipa et al. 2013). In this context, Dock colocalizes with and/or binds to several cell adhesion proteins from the IgCAM superfamily including Rst, one of the genes identified in this screen (see above). Additionally, Dock genetically and biochemically interacts with the Ste20-like serine-threonine kinase Misshapen (Msn) to control motility of photoreceptor growth cones in the developing eye (Ruan et al. 1999). Notably, Msn is required for border cell migration, where it is required for the formation of polarized protrusions and coordinated actomyosin contractility of the cluster (Plutoni et al. 2019). Thus, it will be of interest in the future to determine if Dock, Rst, and Msn interact to control border cell migration.

318 *Atypical cadherins and planar cell polarity genes:* Three genes, *Wnt4*, *ds*, and *ft* encode
319 proteins with annotated roles in both planar cell polarity and cell-cell adhesion (FlyBase; Figure
320 3; Table 2). Wnt4 (human WNT9A) is a conserved secreted protein of the Wnt family, which
321 regulates cell adhesion through recruitment of focal adhesion complexes during the migration of
322 epithelial cells in the pupal ovary (Cohen et al. 2002). We tested four RNAi lines for *Wnt4*, which
323 in total target two independent regions of the gene. Migration defects for the four tested *Wnt4*
324 RNAi lines ranged from 9 to 23% (Figure 3, C, D, I; Table 2). These data suggest a role for Wnt4
325 in regulating border cell movement. Previous studies suggested that Wnt4 participates in
326 establishing planar polarity within the developing eye and wing (Lim et al. 2005; Wu et al. 2013).
327 Indeed, several core planar cell polarity genes including *frizzled* and *dishevelled* regulate border
328 cell migration (Bastock and Strutt 2007). However, recent studies that used multiple gene
329 knockouts now indicate that the Wnt family of proteins, including Wnt4, are not required for
330 *Drosophila* planar cell polarity (Ewen-Campen et al. 2020; Yu et al. 2020). Thus, we favor a role
331 for Wnt4 in the movement and adhesion of border cells, similar to what was found during earlier
332 stages of *Drosophila* ovarian development (Cohen et al. 2002).

333 Ds (human DCHS1) and Ft (human FAT4) encode large protocadherin proteins, each of which
334 has multiple extracellular cadherin repeats (27 for Ds and 34 for Ft) (Fulford and McNeill 2020).
335 Heterophilic binding between Ds and Ft via their extracellular domains is essential for cell-cell
336 communication, particularly in the regulation of tissue growth through Hippo signaling and planar
337 polarization of various tissues (Matakatsu and Blair 2004; Bosveld et al. 2016; Blair and McNeill
338 2018; Fulford and McNeill 2020). Knockdown of *ds* with any of three independent RNAi lines
339 (VDRC 36219, VDRC 4313, and BL 32964) mildly disrupted migration, ranging from 12-14% of
340 border cells failing to reach the oocyte (Figure 3, E, F, J; Table 2). *ds* RNAi border cell clusters

only displayed mild cohesion defects, with 5% of clusters splitting apart (Figure 3E). Two independent RNAi lines that target *ft* (VDRC 108863 and VDRC 9396) also showed consistent though mild migration defects (11-13%), with only a few clusters (3%) splitting apart (Figure 3, G, H, K; Table 2). Interestingly, *ds* is required for the collective directional migration of *Drosophila* larval epidermal cells (LECs) during morphogenesis of the pupal abdominal epithelium (Bischoff 2012; Arata et al. 2017). An imbalance in Ds protein levels between LECs during collective migration is detected by Ft at cell junctions leading to the formation of lamellipodia at the posterior side of the LECs (Arata et al. 2017). Further experiments will be needed to determine if Ft and Ds similarly coordinate protrusions in border cells or regulate some other aspect of border cell collective migration.

**Analysis of regional expression of border cell screen hits in GBM tumors**

Based on the results of the functional *Drosophila* screen, we next sought to link individual genes to invasion in human GBM patient tumors. We first assessed the Ivy GAP database that provides regional RNA expression across anatomically defined regions of tumors ranging from the tumor core to the infiltrating edge (see Methods & Materials). Using this database, we found that NEGR1 and KIRREL3 were specifically enriched in anatomical regions with elevated invasion potential, namely the leading edge (LE) and infiltrating tumor (IT), compared to all other assessed anatomical regions (Figure 4A; Supplementary Table 1). These regions included cellular tumor (CT), perinecrotic zone (PNZ), pseudopalisading cells around necrosis (PAN), hyperplastic blood vessels (HBV), and microvascular proliferation (MP). Additionally, CTNNA2 had significant expression in the LE and IT regions though was expressed in other regions of the tumor (Supplementary Figure 1; Supplementary Table 1). However, we also observed some *Drosophila*

364 screen hits that did not demonstrate regional heterogeneity in terms of expression, such as SYMPK
365 and CTNNA1 (Figure 4B; Supplementary Table 1). Other genes had a mixture of expression
366 profiles across human GBM anatomical regions (CTNNA3, DCHS1, FAT4, KIRREL1,
367 KIRREL2, NCK1; Supplementary Figure 1; Supplementary Table 1). WNT9A was not found in
368 the Ivy GAP database. It is worth noting that this initial validation approach takes advantage of
369 regional differences within the same GBM tumor. Therefore, such GBM anatomical expression
370 surveys may be a better surrogate of cellular invasion than expression in GBM compared to lower-
371 grade or non-neoplastic neural tissue; these latter analyses rely on gene expression in tissue
372 obtained mainly from the core of the tumor and may miss areas of the tumor that undergo active
373 invasion (Supplementary Figures 2 and 3). Nonetheless, we observed a variety of human adhesion
374 ortholog gene-dependent increases or decreases in GBM tumors compared to lower-grade or non-
375 neoplastic neural tissue (Supplementary Figures 2 and 3). Together, these assessments provide a
376 first step in validating novel, conserved molecular mechanisms of GBM invasion for future
377 therapeutic development. Invasive GBM is thought to be driven by CSCs, which can migrate and
378 invade as single cells, finger-like collectives, or as a mixture of migration modes (Cheng et al.
379 2011; Volovetz et al., 2020). Human Rap1a, originally identified in a *Drosophila* screen of
380 collective border cell migration, influences CSC-mediated GBM cell invasion (Aranjuez et al.,
381 2012; Volovetz et al. 2020). Interestingly, knocking down *Sym* and *α-Cat* in the border cells caused
382 the most severe migration and cluster cohesion defects. While the respective human orthologs
383 SYMPK, CTNNA1, and CTNNA2 did not show regional tumor heterogeneity, they are each
384 expressed in GBM tumors and/or are generally elevated in different grades of glioma including
385 GBM (Grade IV; Supplementary Figure 2).
386

## CONCLUSION

GBM, the most common primary malignant brain tumor in adults, is also one of the most lethal (Ostrom et al. 2014; Ostrom et al. 2018). These tumors are highly invasive and possess a self-renewing CSC population. CSCs are highly invasive and can migrate either individually or collectively (Cheng et al. 2011, Volovetz et al. 2020). Here we used a human GBM-informed approach to identify conserved regulators of adhesion during collective cell migration and invasion, particularly focused on testing genes in the border cell model. We identified eight adhesion-related *Drosophila* genes (orthologs of 13 human genes) associated with glioma patient survival. Of the eight adhesion-related *Drosophila* genes found to be essential for collective cell migration, two human orthologs, NEGR1 and KIRREL3 showed significant regional enrichment in the leading edge and infiltrating tumor of human GBM tumors, areas associated with enhanced cell invasion. CTNNA2 was expressed in these invasive regions, though was also expressed at high levels in other regions of the tumor. Knockdown of these eight genes disrupted border cell migration to varying degrees, with two genes *α-cat* and *Sym* significantly disrupting both cohesion of the cluster and successful cell migration. These eight *Drosophila* genes thus represent a starting point to further investigate the specific mechanisms by which these genes regulate normal collective cell migration. Whether the human orthologs function through an adhesion-dependent or -independent manner in GBM tumors needs to be determined with follow up experiments, using both mammalian and non-mammalian models of GBM (Shahzad et al. 2021). Overall, the strategy used in this study has the potential to identify new genes and conserved mechanisms that drive collective cell migration of normal cells and those in invasive cancers such as GBM.

## ACKNOWLEDGMENTS

We thank the Vienna *Drosophila* Resource Center, Harvard Transgenic RNAi Project, and Bloomington *Drosophila* Stock Center for providing flies, and the Developmental Studies Hybridoma Bank at the University of Iowa for providing antibodies used in this study. We thank the Kansas State University College of Veterinary Medicine Confocal Core for use of the Zeiss LSM880 confocal. Thank you to C. Luke Messer, Emily Burghardt and Dr. Yujun Chen. for helpful comments on the manuscript.

## FUNDING

This work was supported in part by NIH R21 CA198254 (J.D.L. and J.A.M.) and by the Johnson Cancer Research Center at Kansas State University through an equipment grant (J.A.M.), an Investigator Research Award (J.A.M.), and a Graduate Student Summer Stipend Award (N.K. and J.A.M.).

## CONFLICT OF INTEREST

The authors declare no conflicts of interest.

## LITERATURE CITED

Aceto N, Bardia A, Miyamoto DT, Donaldson MC, Wittner BS, Spencer JA, Yu M, Pely A, Engstrom A, Zhu H, et al. 2014. Circulating tumor cell clusters are oligoclonal precursors of breast cancer metastasis. Cell. 158(5):1110–1122.

Alhadyian H, Shoaib D, Ward RE. 2021 Apr 19. Septate junction proteins are required for egg elongation and border cell migration during oogenesis in Drosophila. G3 (Bethesda).

Arata M, Sugimura K, Uemura T. 2017. Difference in Dachsous Levels between Migrating Cells Coordinates the Direction of Collective Cell Migration. Developmental Cell. 42(5):479-497.e10.

Aranjuez G, Kudlaty E, Longworth MS, McDonald JA. 2012. On the Role of PDZ Domain-Encoding Genes in Drosophila Border Cell Migration. G3: Genes, Genomes, Genetics. 2(11):1379–1391. doi:10.1534/g3.112.004093.

Bao S, Cagan R. 2005. Preferential adhesion mediated by Hibris and Roughest regulates morphogenesis and patterning in the Drosophila eye. Dev Cell. 8(6):925–935.

Bao S, Wu Q, McLendon RE, Hao Y, Shi Q, et al. 2006. Glioma stem cells promote radioresistance by preferential activation of the DNA damage response. Nature. 444(7120):756–760. doi:10.1038/nature05236.

Bastock R, Strutt D. 2007. The planar polarity pathway promotes coordinated cell migration during Drosophila oogenesis. Development. 134(17):3055–3064.

Ben-Zvi DS, Volk T. 2019. Escort cell encapsulation of Drosophila germline cells is maintained by irre cell recognition module proteins. Biol Open. 8(3).

Bischoff M. 2012. Lamellipodia-based migrations of larval epithelial cells are required for normal closure of the adult epidermis of Drosophila. Dev Biol. 363(1):179–190.

450 Blair S, McNeill H. 2018. Big roles for Fat cadherins. Curr Opin Cell Biol. 51:73–80.

451 Bosveld F, Guirao B, Wang Z, Rivière M, Bonnet I, Graner F, Bellaïche Y. 2016. Modulation of
452 junction tension by tumor suppressors and proto-oncogenes regulates cell-cell contacts.
453 Development. 143(4):623–634.

454 Buday L, Wunderlich L, Tamás P. 2002. The Nck family of adapter proteins: regulators of actin
455 cytoskeleton. Cell Signal. 14(9):723–731.

456 Cai D, Chen S-C, Prasad M, He L, Wang X, Choesmel-Cadamuro V, Sawyer JK, Danuser G,
457 Montell DJ. 2014. Mechanical feedback through E-cadherin promotes direction sensing
458 during collective cell migration. Cell. 157(5):1146–1159.

459 Chaki SP, Rivera GM. 2013. Integration of signaling and cytoskeletal remodeling by Nck in
460 directional cell migration. Bioarchitecture. 3(3):57–63.

461 Chang Y-C, Wu J-W, Hsieh Y-C, Huang T-H, Liao Z-M, Huang Y-S, Mondo JA, Montell D, Jang
462 AC-C. 2018. Rap1 Negatively Regulates the Hippo Pathway to Polarize Directional
463 Protrusions in Collective Cell Migration. Cell Rep. 22(8):2160–2175.

464 Chen J, Li Y, Yu T-S, McKay RM, Burns DK, Kernie SG, Parada LF. 2012. A restricted cell
465 population propagates glioblastoma growth after chemotherapy. Nature. 488(7412):522–
466 526. doi:10.1038/nature11287.

467 Chen Y, Kotian N, Aranjuez G, Chen L, Messer CL, Burtscher A, Sawant K, Ramel D, Wang X,
468 McDonald JA. 2020. Protein phosphatase 1 activity controls a balance between collective
469 and single cell modes of migration. Piotrowski T, Banerjee U, editors. eLife. 9:e52979.

470 Cheng L, Wu Q, Guryanova OA, Huang Z, Huang Q, Rich JN, Bao S. 2011. Elevated invasive
471 potential of glioblastoma stem cells. Biochem Biophys Res Commun. 406(4):643–648.
472 doi:10.1016/j.bbrc.2011.02.123.

473 Cheung KJ, Ewald AJ. 2016. A collective route to metastasis: Seeding by tumor cell clusters.
474 Science. 352(6282):167–169.
475 Cheung KJ, Padmanaban V, Silvestri V, Schipper K, Cohen JD, Fairchild AN, Gorin MA, Verdone
476 JE, Pienta KJ, Bader JS, et al. 2016. Polyclonal breast cancer metastases arise from
477 collective dissemination of keratin 14-expressing tumor cell clusters. PNAS. 113(7):E854–
478 E863.
479 Cohen ED, Mariol M-C, Wallace RMH, Weyers J, Kamberov YG, Pradel J, Wilder EL. 2002.
480 DWnt4 regulates cell movement and focal adhesion kinase during Drosophila ovarian
481 morphogenesis. Dev Cell. 2(4):437–448.
482 Desai R, Sarpal R, Ishiyama N, Pellikka M, Ikura M, Tepass U. 2013. Monomeric α-catenin links
483 cadherin to the actin cytoskeleton. Nat Cell Biol. 15(3):261–273.
484 Ewen-Campen B, Comyn T, Vogt E, Perrimon N. 2020. No Evidence that Wnt Ligands Are
485 Required for Planar Cell Polarity in Drosophila. Cell Rep. 32(10):108121.
486 Finegan TM, Bergstralh DT. 2020. Neuronal immunoglobulin superfamily cell adhesion
487 molecules in epithelial morphogenesis: insights from Drosophila. Philos Trans R Soc Lond
488 B Biol Sci. 375(1809):20190553.
489 Friedl P, Gilmour D. 2009. Collective cell migration in morphogenesis, regeneration and cancer.
490 Nat Rev Mol Cell Biol. 10(7):445–457.
491 Friedl P, Locker J, Sahai E, Segall JE. 2012. Classifying collective cancer cell invasion. Nat Cell
492 Biol. 14(8):777–783.
493 Friedl P, Mayor R. 2017. Tuning Collective Cell Migration by Cell–Cell Junction Regulation. Cold
494 Spring Harb Perspect Biol. 9(4):a029199.

495 Fulford AD, McNeill H. 2020. Fat/Dachsous family cadherins in cell and tissue organisation. Curr
496 Opin Cell Biol. 62:96–103.
497 Garrity PA, Rao Y, Salecker I, McGlade J, Pawson T, Zipursky SL. 1996. Drosophila
498 photoreceptor axon guidance and targeting requires the dreadlocks SH2/SH3 adapter
499 protein. Cell. 85(5):639–650.
500 Gritsenko P, Leenders W, Friedl P. 2017. Recapitulating in vivo-like plasticity of glioma cell
501 invasion along blood vessels and in astrocyte-rich stroma. Histochem Cell Biol.
502 148(4):395–406.
503 Gritsenko PG, Friedl P. 2018. Adaptive adhesion systems mediate glioma cell invasion in complex
504 environments. J Cell Sci. 131(15).
505 Haeger A, Alexander S, Vullings M, Kaiser FMP, Veelken C, Flucke U, Koehl GE, Hirschberg
506 M, Flentje M, Hoffman RM, et al. 2019. Collective cancer invasion forms an integrin-
507 dependent radioresistant niche. Journal of Experimental Medicine. 217(e20181184).
508 Hu Y, Flockhart I, Vinayagam A, Bergwitz C, Berger B, Perrimon N, Mohr SE. 2011. An
509 integrative approach to ortholog prediction for disease-focused and other functional studies.
510 BMC Bioinformatics. 12:357.
511 Ilina O, Campanello L, Gritsenko PG, Vullings M, Wang C, Bult P, Losert W, Friedl P. 2018.
512 Intravital microscopy of collective invasion plasticity in breast cancer. Dis Model Mech.
513 11(9).
514 Janiszewska M, Primi MC, Izard T. 2020. Cell adhesion in cancer: Beyond the migration of single
515 cells. J Biol Chem. 295(8):2495–2505.
516 Johnson RI, Sedgwick A, D'Souza-Schorey C, Cagan RL. 2011. Role for a Cindr-Arf6 axis in
517 patterning emerging epithelia. Mol Biol Cell. 22(23):4513–4526.

518 Kaipa BR, Shao H, Schäfer G, Trinkewitz T, Groth V, Liu J, Beck L, Bogdan S, Abmayr SM,
519 Önel S-F. 2013. Dock mediates Scar- and WASp-dependent actin polymerization through
520 interaction with cell adhesion molecules in founder cells and fusion-competent myoblasts.
521 J Cell Sci. 126(1):360–372.
522 Keon BH, Schäfer S, Kuhn C, Grund C, Franke WW. 1996. Symplekin, a novel type of tight
523 junction plaque protein. J Cell Biol. 134(4):1003–1018.
524 Kim YH, Choi YW, Lee J, Soh EY, Kim J-H, Park TJ. 2017. Senescent tumor cells lead the
525 collective invasion in thyroid cancer. Nat Commun. 8(1):15208.
526 Libanje F, Raingeaud J, Luan R, Thomas Z, Zajac O, Veiga J, Marisa L, Adam J, Boige V, Malka
527 D, et al. 2019. ROCK2 inhibition triggers the collective invasion of colorectal
528 adenocarcinomas. EMBO J. 38(14):e99299.
529 Lim J, Norga KK, Chen Z, Choi K-W. 2005. Control of planar cell polarity by interaction of
530 DWnt4 and four-jointed. genesis. 42(3):150–161.
531 Llimargas M, Strigini M, Katidou M, Karagogeos D, Casanova J. 2004. Lachesin is a component
532 of a septate junction-based mechanism that controls tube size and epithelial integrity in the
533 Drosophila tracheal system. Development. 131(1):181–190.
534 Madsen CD, Hooper S, Tozluoglu M, Bruckbauer A, Fletcher G, Erler JT, Bates PA, Thompson
535 B, Sahai E. 2015. STRIPAK components determine mode of cancer cell migration and
536 metastasis. Nat Cell Biol. 17(1):68–80.
537 Maiden SL, Hardin J. 2011. The secret life of α-catenin: moonlighting in morphogenesis. J Cell
538 Biol. 195(4):543–552.
539 Marcinkevicius E, Zallen JA. 2013. Regulation of cytoskeletal organization and junctional
540 remodeling by the atypical cadherin Fat. Development. 140(2):433–443.

541 Matakatsu H, Blair SS. 2004. Interactions between Fat and Dachsous and the regulation of planar
542 cell polarity in the Drosophila wing. Development. 131(15):3785–3794. McCrea PD, Gu D,
543 Balda MS. 2009. Junctional Music that the Nucleus Hears: Cell–Cell Contact Signaling and
544 the Modulation of Gene Activity. Cold Spring Harb Perspect Biol. 1(4).
545 McGuire SE, Mao Z, Davis RL. 2004. Spatiotemporal Gene Expression Targeting with the
546 TARGET and Gene-Switch Systems in Drosophila. Sci STKE. 2004(220):pl6–pl6.
547 doi:10.1126/stke.2202004pl6.
548 Montell DJ, Yoon WH, Starz-Gaiano M. 2012. Group choreography: mechanisms orchestrating
549 the collective movement of border cells. Nat Rev Mol Cell Biol. 13(10):631–645.
550 Niewiadomska P, Godt D, Tepass U. 1999. DE-Cadherin is required for intercellular motility
551 during Drosophila oogenesis. J Cell Biol. 144(3):533–547.
552 Ostrom QT, Bauchet L, Davis FG, Deltour I, Fisher JL, Langer CE, Pekmezci M, Schwartzbaum
553 JA, Turner MC, Walsh KM, et al. 2014. The epidemiology of glioma in adults: a “state of
554 the science” review. Neuro Oncol. 16(7):896–913. doi:10.1093/neuonc/nou087.
555 Ostrom QT, Cote DJ, Ascha M, Kruchko C, Barnholtz-Sloan JS. 2018. Adult Glioma Incidence
556 and Survival by Race or Ethnicity in the United States From 2000 to 2014. JAMA Oncol.
557 4(9):1254–1262. doi:10.1001/jamaoncol.2018.1789.
558 Padmanaban V, Krol I, Suhail Y, Szczerba BM, Aceto N, Bader JS, Ewald AJ. 2019. E-cadherin
559 is required for metastasis in multiple models of breast cancer. Nature. 573(7774):439–444.
560 Plutoni C, Keil S, Zeledon C, Delsin LEA, Decelle B, Roux PP, Carréno S, Emery G. 2019.
561 Misshapen coordinates protrusion restriction and actomyosin contractility during collective
562 cell migration. Nat Commun. 10(1):3940.

563 Rao Y, Zipursky SL. 1998. Domain requirements for the Dock adapter protein in growth- cone
564 signaling. PNAS. 95(5):2077–2082.
565 Raza Q, Choi JY, Li Y, O'Dowd RM, Watkins SC et al., 2019. Evolutionary rate covariation
566 analysis of E-cadherin identifies Raskol as a regulator of cell adhesion and actin dynamics
567 in Drosophila. PLOS Genetics. 15(2):e1007720.
568 Ruan W, Pang P, Rao Y. 1999. The SH2/SH3 adaptor protein dock interacts with the Ste20-like
569 kinase misshapen in controlling growth cone motility. Neuron. 24(3):595–605.
570 Saadin A, Starz-Gaiano M. 2016. Circuitous Genetic Regulation Governs a Straightforward Cell
571 Migration. Trends Genet. 32(10):660–673.
572 Sarpal R, Pellikka M, Patel RR, Hui FYW, Godt D, Tepass U. 2012. Mutational analysis supports
573 a core role for Drosophila α-catenin in adherens junction function. J Cell Sci. 125(Pt 1):233–
574 245.
575 Sawant K, Chen Y, Kotian N, Preuss KM, McDonald JA. 2018. Rap1 GTPase promotes
576 coordinated collective cell migration in vivo. MBoC. 29(22):2656–2673.
577 Scarpa E, Mayor R. 2016. Collective cell migration in development. J Cell Biol. 212(2):143–155.
578 Shahzad U, Taccone MS, Kumar SA, Okura H, Krumholtz S et al. 2021. Modeling human brain
579 tumors in flies, worms, and zebrafish: From proof of principle to novel therapeutic targets.
580 Neuro Oncol. 23(5):718–731. doi:10.1093/neuonc/noaa306.
581 Stark K, Crowe O, Lewellyn L. 2021. Precise levels of the Drosophila adaptor protein Dreadlocks
582 maintain the size and stability of germline ring canals. J Cell Sci. 134(8).
583 Stuelten CH, Parent CA, Montell DJ. 2018. Cell motility in cancer invasion and metastasis:
584 insights from simple model organisms. Nat Rev Cancer. 18(5):296–312.

585 Sullivan KD, Steiniger M, Marzluff WF. 2009. A core complex of CPSF73, CPSF100, and
586 Symplekin may form two different cleavage factors for processing of poly(A) and histone
587 mRNAs. Mol Cell. 34(3):322–332. .
588 Tatomer DC, Rizzardi LF, Curry KP, Witkowski AM, Marzluff WF, Duronio RJ. 2014.
589 Drosophila Symplekin localizes dynamically to the histone locus body and tricellular
590 junctions. Nucleus. 5(6):613–625.
591 Tang Z, Li Chenwei, Kang B, Gao G, Li Cheng, Zhang Z. 2017. GEPIA: a web server for cancer
592 and normal gene expression profiling and interactive analyses. Nucleic Acids Res.
593 45(W1):W98–W102. doi:10.1093/nar/gkx247.
594 Te Boekhorst V, Friedl P. 2016. Plasticity of Cancer Cell Invasion-Mechanisms and Implications
595 for Therapy. Adv Cancer Res. 132:209–264.
596 Te Boekhorst V, Preziosi L, Friedl P. 2016. Plasticity of Cell Migration In Vivo and In Silico.
597 Annu Rev Cell Dev Biol. 32:491–526.
598 Valer FB, Machado MCR, Silva-Junior RMP, Ramos RGP. 2018. Expression of Hbs, Kirre, and
599 Rst during Drosophila ovarian development. Genesis. 56(9):e23242.
600 Volovetz J, Berezovsky AD, Alban T, Chen Y, Lauko A, Aranjuez GF, Burtscher A, Shibuya K,
601 Silver DJ, Peterson J, et al. 2020. Identifying conserved molecular targets required for cell
602 migration of glioblastoma cancer stem cells. Cell Death Dis. 11(2):152.
603 Wang X, Enomoto A, Asai N, Kato T, Takahashi M. 2016. Collective invasion of cancer:
604 Perspectives from pathology and development. Pathol Int. 66(4):183–192.
605 Wu J, Roman A-C, Carvajal-Gonzalez JM, Mlodzik M. 2013. Wg and Wnt4 provide long-range
606 directional input to planar cell polarity orientation in Drosophila. Nat Cell Biol. 15(9):1045–
607 1055.

608 Yoshida H, Cheng W, Hung J, Montell D, Geisbrecht E, Rosen D, Liu J, Naora H. 2004. Lessons
609 from border cell migration in the Drosophila ovary: A role for myosin VI in dissemination
610 of human ovarian cancer. PNAS. 101(21):8144–8149.
611 Yu JJS, Maugarny-Calès A, Pelletier S, Alexandre C, Bellaiche Y, Vincent J-P, McGough IJ.
612 2020. Frizzled-Dependent Planar Cell Polarity without Secreted Wnt Ligands.
613 Developmental Cell. 54(5):583-592.e5.
614
615

## FIGURE LEGENDS

**Figure 1.** Screen to identify conserved GBM-associated adhesion genes in collective cell migration. (A-C) Migration of wild type border cells in stage 9 and 10 egg chambers. *c306*-GAL4 drives nuclear GFP (UAS-nls.GFP, green) in egg chambers labelled with Armadillo (magenta) to show cell membranes and nuclei stained for DAPI (grey). Arrowheads indicate the position of the border cell cluster within the egg chamber during migration stages: pre-migration (A), mid-migration (B), and end-migration (C). (D-E) Knockdown of *E-cadherin* by RNAi (*c306*-GAL4 tsGAL80/+; +/UAS-E-cadherin RNAi line v103962) in border cells disrupts migration and cluster cohesion at stage 10. Arrowheads indicate border cell clusters and split clusters. (F) Schematic overview of the RNAi screening approach in border cells. (G) Experimental flow chart used to identify novel GBM-associated adhesion genes through *Drosophila* and human glioma databases.

**Figure 2.** Cell adhesion and cell junction genes whose RNAi knockdown impairs border cell migration. (A-L) Stage 10 egg chambers expressing RNAi for the indicated genes (or control) in border cells labeled for E-cadherin (red), a cell membrane and adhesion marker, Singed (green), which is highly expressed in and marks border cells, and DAPI to label all cell nuclei (blue). Two images are shown to indicate the general extent of phenotypes with RNAi knockdown for each gene. White arrowheads show the position of border cell clusters; the scale bar (A, B) indicates the image magnification for all images in the figure. Anterior is to the left. (A and B) Border cells expressing the control, *mCherry* RNAi, reach the oocyte at stage 10. (C-L) RNAi knockdown of *α-Catenin/α-Cat* (C and D, line v107298), *Symplekin/Sym* (E, line v33470; F, line v33469), *Lachesin/Lac* (G and H, line BL28940), *Roughest/Rst* (I and J, line v27223) and *Dock* (K, line

v37524; L, line BL27728) driven by *c306*-GAL4 tsGAL80 disrupts the collective migration of border cells. The average percentage of egg chambers with border cell cluster splitting defects (% splitting) from the RNAi line with the strongest migration defect is indicated. (M-Q) Quantification of the extent of border cell migration (no migration, red; partial migration, blue; complete migration, green) in stage 10 egg chambers expressing the indicated RNAi lines for *α-Cat* (M), *Sym* (N), *Lac* (O), *Rst* (P) and *Dock* (Q) along with the matched control *mCherry* RNAi. Error bars represent SEM for three trials, $n \geq 30$ egg chambers in each trial. *$p<0.05$; **$p<0.005$; ***$p<0.001$, unpaired two-tailed t test.

**Figure 3.** Atypical cadherins and planar cell polarity genes whose RNAi knockdown impairs border cell migration. (A-H) Stage 10 egg chambers expressing RNAi for the indicated genes (or control) in border cells labeled for E-cadherin (red), a cell membrane and adhesion marker, Singed (green), which is highly expressed in border cells, and DAPI to label all cell nuclei (blue). Two images are shown to indicate the general extent of phenotypes with RNAi knockdown for each gene. White arrowheads show the position of border cell clusters; the scale bar (A, B) indicates the image magnification for all images in the figure. Anterior is to the left. (A and B) Border cells expressing the control, *mCherry* RNAi, reach the oocyte at stage 10. (C-H) RNAi knockdown of *Wnt4* (C and D, line v38011), *Dachsous/ds* (E, line 32964; F, line v4313) and *Fat/ft* (G and H, line BL28940) driven by *c306*-GAL4 tsGAL80 disrupts the collective migration of border cells. The average percentage of egg chambers with border cell cluster splitting defects from the RNAi line with the strongest migration defect is indicated. (I-K) Quantification of border cell migration (no migration, red; partial migration, blue; complete migration, green) in stage 10 egg chambers expressing the indicated RNAi lines for *Wnt4* (I), *ds* (J), and *ft* (K) along with the matched control

662 *mCherry* RNAi. Error bars represent SEM for three trials, n ≥30 egg chambers in each trial.
663 *p<0.05; **p<0.005; ***p<0.001, unpaired two-tailed t test.
664
665 **Figure 4.** Regional expression of representative human ortholog adhesion genes in GBM patient
666 tumors. (A) Expression of human orthologs of adhesion genes neuronal growth regulator 1
667 (NEGR1) and kirre like nephrin family adhesion molecule 3 (KIRREL3) is significantly enriched
668 in the leading edge (LE) and infiltrating tumor (IT) compared to other tumor regions, including
669 the cellular tumor (CT), perinecrotic zone (PNZ), pseudopalisading cells around necrosis (PAN),
670 hyperplastic blood vessels (HBV), and microvascular proliferation (MP). (B) In contrast,
671 expression of human orthologs symplekin (SYMPK) and catenin alpha 1 (CTNNA1) demonstrated
672 little to no significant change when comparing different regions of tumor. Data from the Ivy GAP
673 are shown as mean expression +/- SD across GBM tumor regions. Statistics are shown in
674 Supplementary Table 1: *p<0.05; **p<0.01; ***p<0.001, one way ANOVA with Tukey HSD.
675
676 **Supplementary Figure 1.** Regional expression of human ortholog adhesion genes in GBM patient
677 tumors for additional human genes. See Figure 4 legend for abbreviations of the tumor regions.
678 Data from the Ivy GAP are shown as mean expression +/- SD across GBM tumor regions. Statistics
679 are shown in Supplementary Table 1: *p<0.05; **p<0.01; ***p<0.001, one way ANOVA with
680 Tukey HSD.
681
682 **Supplementary Figure 2.** Expression of human ortholog adhesion genes across glioma tumor
683 grade. Box plots of mRNA expression obtained from the TCGA database in grade II (n=226),

684 grade III (n=244), and grade IV (n=150) patient gliomas. *p<0.05; **p<0.01; ***p<0.001, one
685 way ANOVA with Tukey HSD.
686
687 **Supplementary Figure 3.** Expression of human ortholog adhesion genes in GBM compared to
688 non-tumor brain tissue. Box plots of mRNA expression obtained from the GEPIA database in non-
689 tumor (n=207) and GBM tumor (n=163). *p<0.01.
690
691 **Supplementary Table 1.** Statistics for the Ivy GAP regional gene expression for all human
692 adhesion gene orthologs. Graphed data are shown in Figure 4 and Supplementary Figure 1.

693 **Table 1.** *Drosophila* and human brain tumor-associated adhesion genes.

| *Gene name (Drosophila)* | *Human ortholog* | *DIOPT score out of 15* | *Best score* | *Best reverse score* | *Glioma patient survival* |
|---|---|---|---|---|---|
| *alpha-Catenin* | CTNNA1 | 12 | No | Yes | Negative |
| | CTNNA2 | 13 | Yes | Yes | ND |
| | CTNNA3 | 7 | No | Yes | Positive |
| *CAP* | SORBS1 | 5 | No | Yes | Positive |
| *Caskin* | CASKIN1 | 4 | Yes | Yes | Positive |
| | CASKIN2 | 4 | Yes | Yes | Positive |
| *CG3770* | LHFPL2 | 12 | Yes | Yes | Negative |
| *CG45049* | PERP | 10 | No | Yes | Negative |
| *Dachsous* | DCHS1 | 11 | Yes | Yes | Negative |
| *Dock* | NCK1 | 14 | Yes | Yes | Negative |
| *Fat* | FAT4 | 13 | Yes | Yes | Positive |
| *G protein alpha i* | GNAI2 | 11 | No | Yes | Negative |
| | GNAZ | 5 | No | Yes | Positive |
| *G protein alpha o* | GNAI3 | 3 | No | No | Negative |
| | GNAT3 | 3 | No | No | Positive |
| *Gliotactin* | NLGN2 | 5 | Yes | No | Positive |
| *Lachesin* | LSAMP | 5 | No | No | Positive |
| | NEGR1 | 9 | Yes | Yes | Positive |
| *Liprin-alpha* | PPFIA1 | 11 | No | Yes | Negative |
| *Lowfat* | LIX1L | 13 | Yes | Yes | Positive |
| | LIX1 | 7 | No | Yes | Positive |
| *Mesh* | SUSD2 | 13 | Yes | Yes | Negative |
| *Parvin* | PARVA | 14 | Yes | Yes | Positive |
| | PARVB | 13 | No | Yes | Positive |
| *Roughest* | KIRREL1 | 13 | Yes | Yes | Negative |

| ***Gene name (Drosophila)*** | ***Human ortholog*** | ***DIOPT score out of 15*** | ***Best score*** | ***Best reverse score*** | ***Glioma patient survival*** |
|---|---|---|---|---|---|
| | KIRREL3 | 12 | No | Yes | Negative |
| | KIRREL2 | 11 | No | Yes | Negative |
| *schizo* | IQSEC2 | 12 | No | Yes | Positive |
| *Shroom* | SHROOM1 | 2 | No | Yes | Negative |
| | SHROOM3 | 8 | Yes | Yes | Negative |
| *Symplekin* | SYMPK | 14 | Yes | Yes | Negative |
| *Vulcan* | DLGAP1 | 7 | Yes | Yes | Positive |
| | DLGAP2 | 6 | No | Yes | Positive |
| *Wnt4* | WNT9A | 4 | No | Yes | Positive |
| *Wunen* | PLPP2 | 9 | No | No | Negative |

694

695 ND, not determined

696 Human orthologs of adhesion genes obtained from the *Drosophila* RNAi Screening Center
697 Integrative Ortholog Prediction Tool (DIOPT). DIOPT score depicts the number of alignment
698 tools that support an orthologous gene-pair. Best score (yes or no) indicates if the given
699 score is the highest score. Glioma patient survival (positive or negative) is listed for each gene
700 from The Cancer Genome Atlas (TCGA) and NCI REMBRANDT.

701

**Table 2.** Results of the primary and secondary RNAi screens in border cells.

| Gene | RNAi | Stock center | Construct ID | Migration defect (Primary screen) | Migration defect (Secondary screen): Mean ± [SD] |
|---|---|---|---|---|---|
| ***alpha-catenin (α-cat)*** | **20123#** | **VDRC** | **GD8808** | **89%** | **76% ± 0.07#** |
| | **107298** | **VDRC** | **KK107916** | **86%** | **66% ± 0.05** |
| | **40882** | **VDRC** | **GD8808** | **73%** | ND |
| *CAP* | 106309 | VDRC | KK107936 | 0.80% | 2% ± 0.01 |
| | 19054 | VDRC | GD8545 | 7% | 4% ± 0.01 |
| | 30506 | BL | HMS05250 | 11% | 4% ± 0.03 |
| | 36663 | BL | HMS01551 | 6.30% | 5% ± 0.01 |
| *Caskin* | 24526 | VDRC | GD7723 | 11% | 9% ± 0.02 |
| | 25222 | VDRC | GD7723 | 10% | 9% ± 0.00 |
| *CG3770* | 4064 | VDRC | GD2223 | 8% | 9% ± 0.01§ |
| | 103556 | VDRC | KK101078 | 26% | 2% ± 0.01 |
| | 61262 | BL | HMJ2304 | 9% | 8% ± 0.01 |
| *CG45049* | 102985 | VDRC | KK112983 | 13% | 4% ± 0.01 |
| | 102025 | VDRC | KK110412 | 8% | 8% ± 0.01 |
| | 32403 | VDRC | GD8606 | 20% | 12% ± 0.02 |
| | 9673 | VDRC | GD3956 | 8% | 8%§ |
| ***Dachsous (ds)*** | **36219** | **VDRC** | **GD14350** | **5%** | **14 ± 0.02** |
| | **4313** | **VDRC** | **GD2646** | **11%** | **12% ± 0.07** |
| | **32964** | **BL** | **HMS00759** | **ND** | **13% ± 0.05** |
| ***Dreadlocks (dock)*** | **37524** | **VDRC** | **GD4034** | **9%** | **19% ± 0.03** |
| | **37525** | **VDRC** | **GD4035** | **11%** | **NA** |
| | **107064** | **VDRC** | **KK102500** | **5%** | **4% ± 0.04** |
| | **27228** | **BL** | **JF02810** | **8%** | **13% ± 0.02** |
| ***Fat (ft)*** | **108863** | **VDRC** | **KK101190** | **11%** | **11% ± 0.04** |
| | **9396** | **VDRC** | **GD881** | **8%** | **11% ± 0.02** |
| *G protein alpha i subunit* | 40890 | BL | HMS02138 | 20% | 2% ± 0.02 |
| | 31133 | BL | JF0168 | 12% | 3% ± 0.02 |
| | 28150 | VDRC | GD12576 | 5% | 5% ± 0.01 |
| *G protein alpha o subunit* | 34653 | BL | HMS01129 | 4% | 3% ± 0.04 |
| | 34924 | BL | HMS01273 | 16% | 2% ± 0.01 |
| | 110552 | VDRC | KK109018 | 21% | 3% ± 0.01 |
| | 19124 | VDRC | GD8640 | 6% | 15% ± 0.06 |
| *Gliotactin* | 37115 | VDRC | GD1735 | 9% | 10% ± 0.01 |

| Gene | RNAi | Stock center | Construct ID | Migration defect (Primary screen) | Migration defect (Secondary screen): Mean ± [SD] |
|---|---|---|---|---|---|
| | 37116 | VDRC | GD1735 | 12% | 6% ± 0.02 |
| | 107258 | VDRC | KK105971 | 8% | 2% ± 0.03 |
| | 38284 | BL | HMS01737 | 10% | 1% ± 0.01 |
| | 58115 | BL | HMJ22052 | 10% | 3% ± 0.04 |
| ***Lachesin (Lac)*** | **35524** | **VDRC** | **GD 12649** | **15%** | **10% ± 0.02** |
| | **107450** | **VDRC** | **KK 107469** | **17%** | **5% ± 0.03** |
| | **38536** | **BL** | **HMS01756** | **23%** | **5% ± 0.02** |
| | **28940** | **BL** | **HM05151** | **ND** | **10% ± 0.01** |
| *Liprin-alpha* | 106588 | VDRC | KK10116 | 6% | 5% ± 0.05 |
| | 51707 | VDRC | GD7232 | 14% | 7% ± 0.01 |
| | 53868 | BL | HMC03183 | 19% | 5% ± 0.06 |
| *Lowfat* | 32145 | VDRC | GD7934 | 5% | ND |
| | 32146 | VDRC | GD7934 | 3% | ND |
| | 107630 | VDRC | KK102118 | 9.4% | ND |
| | 28755 | BL | JF03183 | 3.5% | ND |
| *Mesh* | 40940 | VDRC | GD3139 | 16% | 3% ± 0.04 |
| | 6867 | VDRC | GD3140 | 6% | NA |
| *Parvin* | 11670 | VDRC | GD3687 | 7.40% | 8% ± 0.01 |
| | 105356 | VDRC | KK102567 | 5% | 2% ± 0.04 |
| | 42831 | BL | HMS02523 | 19% | 3% ± 0.02 |
| ***Roughest (rst)*** | **27223** | **VDRC** | **GD14475** | **22%** | **16% ± 0.03** |
| | **27225** | **VDRC** | **GD14475** | **9.6%** | **11% ± 0.01** |
| | **951** | **VDRC** | **GD86** | **5%** | **4% ± 0.04** |
| | **28672** | **BL** | **JF03087** | **ND** | **10% ± 0.01** |
| *Schizo* | 36625 | VDRC | GD14895 | 7% | 13% ± 0.03 |
| | 36627 | VDRC | GD14895 | 1.50% | NA |
| | 106168 | VDRC | KK103616 | 14% | 4% ± 0.03 |
| | 39060 | BL | HMS01980 | 5% | 3% ± 0.01 |
| *Shroom* | 47147 | VDRC | GD16363 | 6% | 5% ± 0.005 |
| | 100672 | VDRC | KK106863 | 34% | 7% ± 0.04 |
| | 107966 | VDRC | KK108450 | 9.7% | 7% ± 0.02 |
| | 40942 | BL | HMS02190 | 7.4% | 7% ± 0.07 |
| ***Symplekin (Sym)*** | **33469** | **VDRC** | **GD9722** | **14%** | **23% ± 0.1** |
| | **33470** | **VDRC** | **GD9722** | **23%** | **32% ± 0.02** |
| | **39041** | **BL** | **HMS01961** | **8%** | **6% ± 0.01** |

| Gene | RNAi | Stock center | Construct ID | Migration defect (Primary screen) | Migration defect (Secondary screen): Mean ± [SD] |
|---|---|---|---|---|---|
| *Vulcan* | 46229 | VDRC | GD16319 | 14% | 3% ± 0.05 |
| | 46230 | VDRC | GD16319 | 10% | 6% ± 0.01 |
| | 40925 | BL | HMS02173 | 4% | 10% ± 0.03 |
| | | | | | |
| ***Wnt4*** | **38011** | **VDRC** | **GD5347** | **23%** | **24%** |
| | **38010** | **VDRC** | **GD5347** | **7%** | **12% ± 0.02** |
| | **104671** | **VDRC** | **KK102348** | **11%** | **13% ± 0.06** |
| | **29442** | **BL** | **JF03378** | **10%** | **9% ± 0.01** |
| | | | | | |
| *Wunen* | 51090 | VDRC | GD15706 | 5.1% | ND |
| | 51091 | VDRC | GD15706 | 7% | ND |
| | 6446 | VDRC | GD1640 | 7.6% | ND |
| | | | | | |
| *mCherry* | 35785 | BL | VALIUM20-mCherry | 2-11% | 3% ± 0.02 |

703 ND, not determined; NA, not available; SD, standard deviation; §, RNAi line tested in two trials
704 (stock dead or no longer available at the stock center); #, data from Chen et al., 2020.

705 RNAi stock numbers, source of RNAi line, and construct IDs for the 23 candidate genes from the
706 screen. Primary screen results indicate percentage of stage 10 egg chambers with migration defects
707 for each RNAi line of the corresponding gene. Secondary screen results include mean migration
708 defects for each RNAi line from three trials along with the standard deviation. Genes considered
709 as "hits" from the screen are highlighted in bold text.

710

Figure 1

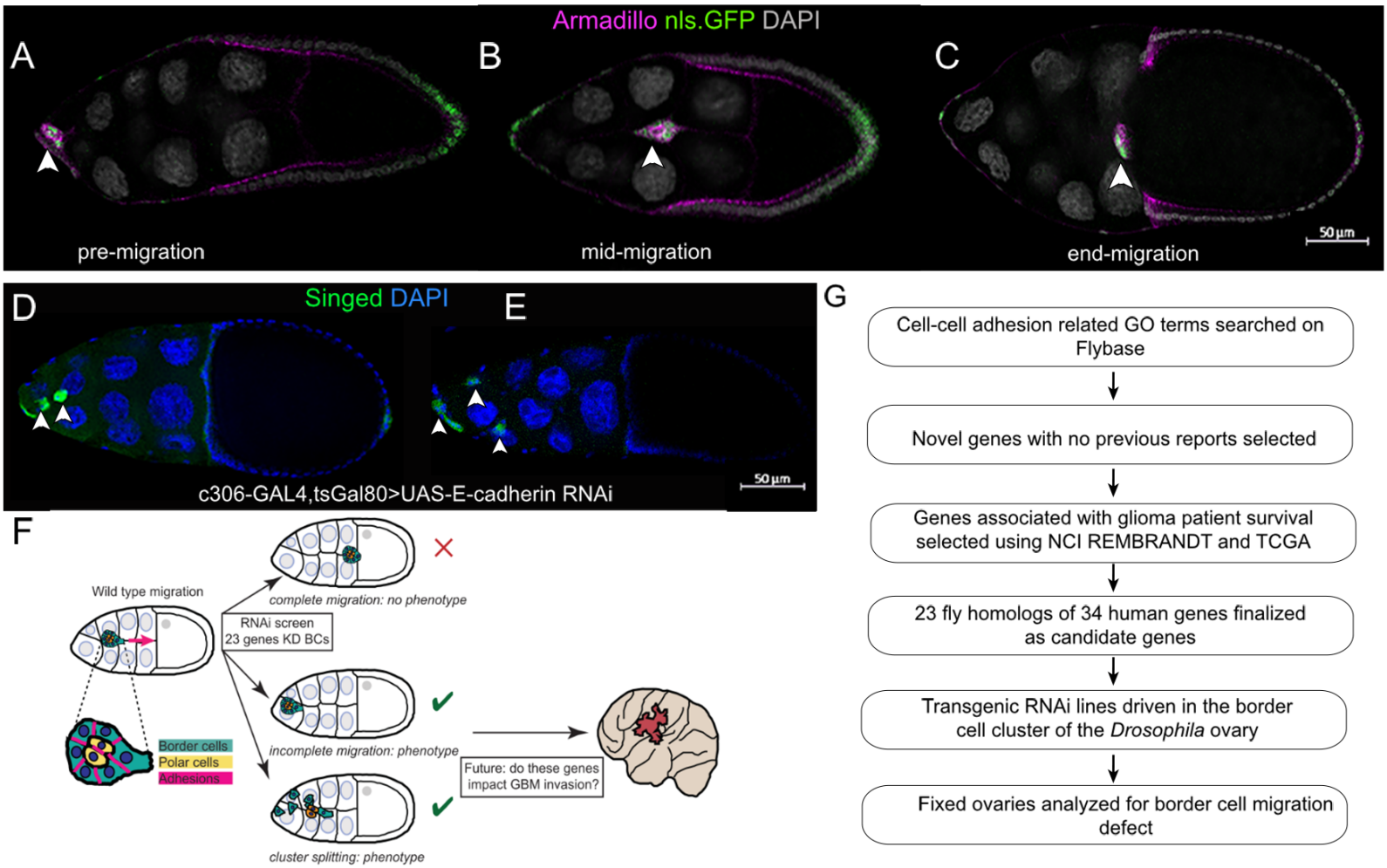

Figure 2

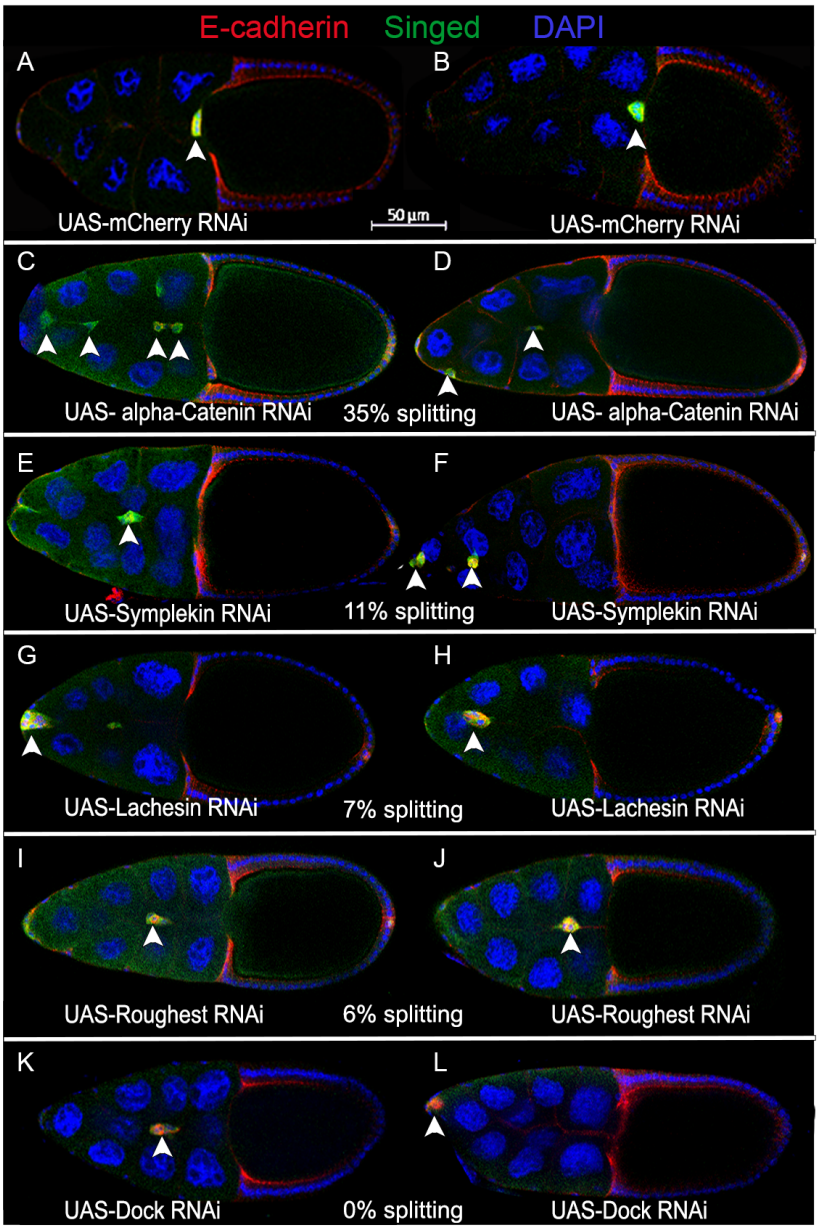


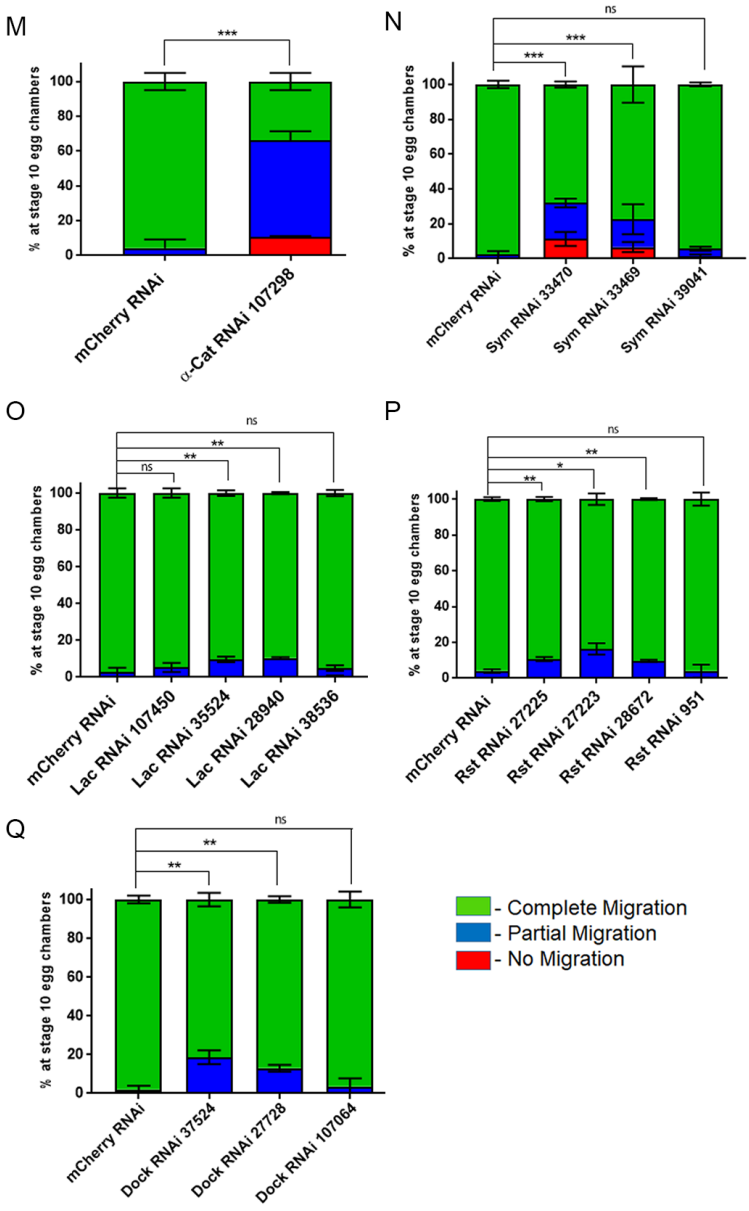

# Figure 3

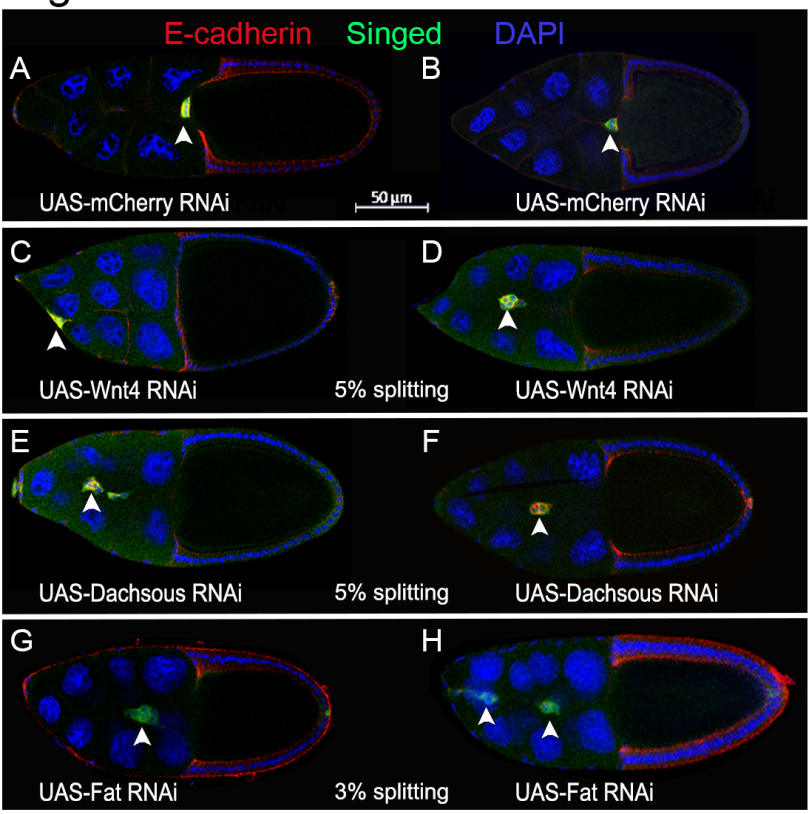


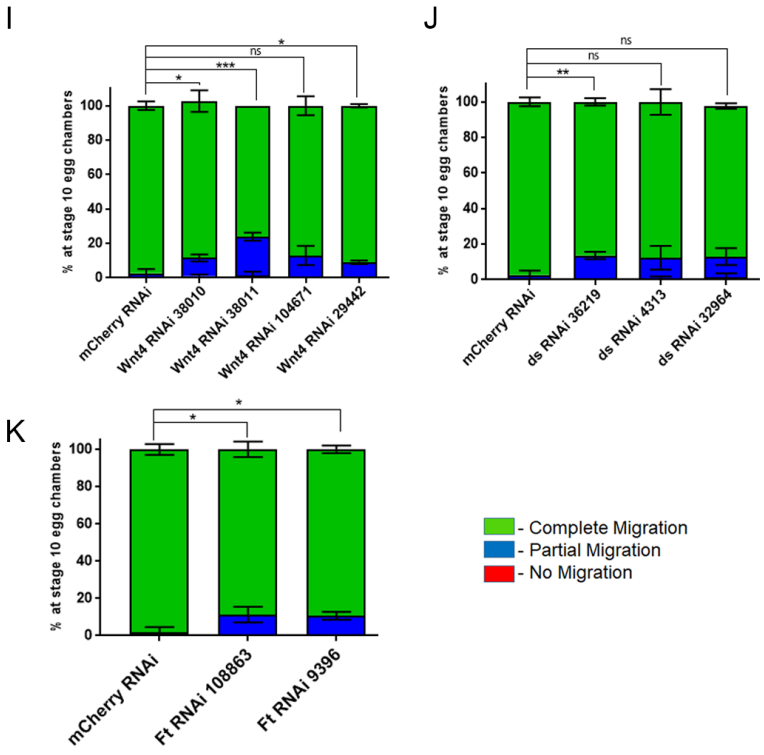

# Figure 4